Research Square

Preprints are preliminary reports that have not undergone peer review.
They should not be considered conclusive, used to inform clinical practice,
or referenced by the media as validated information.

Solvents Adjusted Pure Phase CoCO3 as Anodes for High Cycle Stability

Liming Liu
Harbin Institute of Technology
X.X. Huang (swliza@hit.edu.cn)
Harbin Institute of Technology
Zengyan Wei
Harbin Institute of Technology
Xiaoming Duan
Harbin Institute of Technology
Bo Zhong
Harbin Institute of Technology - Weihai
Long Xia
Harbin Institute of Technology - Weihai
Tao Zhang
Harbin Institute of Technology - Weihai
Huatao Wang
Harbin Institute of Technology - Weihai
Dechang Jia
Harbin Institute of Technology
Yu Zhou
Harbin Institute of Technology
Rui Zhang
Hunan University

Research Article

Keywords: Lithium ion battery, Cobalt carbonate, Solvothermal method, Morphological control, Solvent, Pure phase

Posted Date: July 15th, 2020

DOI: https://doi.org/10.21203/rs.3.rs-41200/v1

License: This work is licensed under a Creative Commons Attribution 4.0 International License.
Read Full License

Version of Record: A version of this preprint was published at Journal of Advanced Ceramics on April 15th, 2021. See the published version at https://doi.org/10.1007/s40145-020-0453-y.

Abstract

$CoCO_3$ with high theoretical capacity has been considered as a candidate anode for the next generation of lithium-ion batteries. However, the electrochemical characteristics of $CoCO_3$ itself, especially the cycle stability under high current density, hindering its application. Herein, pure phase $CoCO_3$ particles with different particle and pore sizes were prepared by adjusting the solvents. $CoCO_3$ synthesized with diethylene glycol (DG-CC) as the reaction solvent shows the best electrochemical performance for the particle size of about 0.85 μm, which because the small primary particle size within and the mesopores maintain the structural stability. A high specific capacity of after 1000 cycles was achieved, and an excellent capacity retention was presented. The capacity provided by different electrochemical reactions and the impedance of DG-CC under different cycles were further compared. Those results provide an important reference for the structural design and stable cycle performance of pure $CoCO_3$.

1. Introduction

Out of the concern for energy and environment, lithium-ion batteries (LIBs) have been widely studied because of their high energy density, low pollution and compatibility with existing equipment [1–3]. In the aspect of anode materials, it is expected that the commercially used graphite can be replaced because of its rather low specific capacity (372 mAh/g) and the hidden danger of lithium dendrite in the process of charge and discharge [4]. The conversion reaction materials [5], such as transition metal oxides (TMOs) and transition metal carbonates (TMCs), have attracted wide attentions due to their higher specific capacity [6–8] and better security than intercalation type anodes [9–12]. However, TMCs show two obvious advantages over TMOs as follows: (1) Easier preparation technology. carbonate is often used as the precursor of oxide, which means that the utilization of carbonate can bring about shortening technological process and cost reduction. (2) Improved properties. TMCs have even higher specific capacity owing to an additional step of lithium storage reaction provided by CO_3^{2-} [13–16]. Among the carbonates, $CoCO_3$ has a high theoretical capacity (1577 mAh/g) and the electrochemical reaction process of $CoCO_3$ has been described by the two-step equation [17]:

$$CoCO_3 + 2Li^+ + 2e^- \leftrightarrow Co + Li_2CO_3 \quad (1)$$

$$Li_2CO_3 + (4 + 0.5x)Li^+ + (4 + 0.5x)e^- \leftrightarrow 3Li_2O + 0.5Li_xC_2 \ (x = 0, 1, 2) \quad (2)$$

In addition, some additional structural designs based on cobalt carbonate as the main active material are carried out to further improve the electrochemical properties [18–22]. Common strategies are (1) preparing composites with carbon material or conductive polymer [17, 23, 24], (2) controlling the shape of $CoCO_3$ particles by morphology directing agent [25], (3) doping of other elements in $CoCO_3$ [26]. However, these strategies such as doping and compounding themselves create additional problems. Since the added carbon materials have lower tap density and provide less capacity, the energy density of the overall composites is whittled down. In addition, these strategies inevitably lead to additional raw materials and

tedious process procedures, thus increased manufacturing costs [27–30]. In a nutshell, the particle structure is considered to be one of the key factors to change the performance of an anode [31]. At present, almost all the preparation methods of cobalt carbonate are hydrothermal or solvothermal method, this suggests that solvent plays an important role in controlling the structure of particles.

Herein, a facile solvothermal route with different solvents was achieved, thus three kinds of bare $CoCO_3$ particles with generally consistent structure but different particle and pore sizes were prepared. Corresponding to the applied solvents diethylene glycol, glycol and water, the products are respectively named as DG-CC, EG-CC and DW-CC. As a result, the cobalt carbonate prepared from diethylene glycol (DG-CC) has a high specific capacity of 690.7 mAh/g at 1 A/g after 1000 cycles, and a high capacity retention with 92.45%. In fact, it is very rare for a pure cobalt carbonate electrode to have such a stable capacity after 1000 cycles. The structure of the particles adjusted by solvent has an important effect on electrochemical performance. Such an example in our work may provide some reference for the structural design of various anode materials in LIBs.

2. Experimental

2.1. Synthesis of DG-CC, EG-CC and DW-CC

Three cobalt carbonate samples (DG-CC, EG-CC and DW-CC) were obtained by solvothermal method with different solvents (diethylene glycol, ethylene glycol and deionized water, respectively). Typically, 1 mmol $Co(Ac)_2{\cdot}4H_2O$ and 10 mmol NH_4HCO_3 were dissolved in a total of 30 ml of solvent at room temperature. By applying repeated ultrasound and agitation, the solute can be dissolved as soon as possible. After the reactants were completely dissolved, the red solution was transferred to a 45 mL Teflon-lined stainless-steel autoclave and maintained at 200 ℃ for 15 h. All solvothermal products were wash by centrifugation with deionized water and ethanol three times each to remove impurities. After dried at 60 °C, DG-CC, EG-CC and DW-CC were prepared.

2.2. Material characterization

X-ray diffraction (XRD) patterns of three cobalt carbonate samples were obtained by a D&A25ADVANCE using Cu Kα radiation. The morphologies of as-prepared $CoCO_3$ samples were examined with a FEI Quanta 200F and a JEM-2100. The thermogravimetric analysis (TGA) was performed on a DTG-60H thermal analyzer under air flow at a rate of 10 ℃/min. Chemical state information was studied by using the X-ray photoelectron spectroscopy (XPS) measurement performed on an ESCALAB 250Xi. The specific surface area and pore size distribution were determined based on Brunauer-Emmett-Teller (BET) and Barrett Joyner-Halenda model, respectively.

2.3 Electrochemical characterization

The $CoCO_3$ electrodes were prepared by laminating the mixed slurry composed of an 80 wt.% $CoCO_3$, 10 wt.% acetylene black, and 10 wt.% polyvinylidene fluoride. After the slurry was mixed evenly, it was coated

on copper foils, and these foils were cut into discs of 14 mm in diameter. After dried in a vacuum oven at 110 °C overnight, the loading density of these electrodes is around 1.5 mg cm^{-2}. The electrodes were assembled into CR2032 coin-cells in an argon filled glovebox, with Li foil as the counter electrode and a microporous polyethylene film (Celgard 2400) as the separator. The electrolyte was 1 M $LiPF_6$ dissolved in a 1 : 1 : 1 mixture of ethylene carbonate, diethyl carbonate, and dimethyl carbonate. The assembled cells were charged and discharged with a voltage range of 0.01–3 V using a cell test system (LAND CT2001A). Cyclic voltammetry (CV) curves and electrochemical impedance spectroscopy (EIS) data were measured on a CHI760E electrochemical workstation operated in the voltage range of 0.01–3 V at a scan rate of 1×10^{-4} V s^{-1} and in the frequency range of 0.01–100 kHz, respectively.

3. Results And Discussion

XRD pattern is shown in Fig. 1, in which DG-CC, EG-CC and DW-CC show the same diffraction peaks. All the diffraction peaks are matched to the standard peaks of $CoCO_3$ (JCPDS No.11–0692), and none impurity phase is observed in these samples. TGA curves (Fig. S1, Supporting Information) demonstrated the thermal behaviors of the $CoCO_3$ samples. The curves first undergo a slow decline, corresponding to the evaporation of water in these materials. In the period of 250–400 ℃, all of the $CoCO_3$ samples lost ~ 33.0% mass, which is consistent with Eq. (3).

$$6CoCO_3 + O_2 \rightarrow 2Co_3O_4 + 6CO_2 \quad (3)$$

XPS spectra of DG-CC, EG-CC and DW-CC are displayed in Fig. S2 (Supporting Information). Because DG-CC, EG-CC and DW-CC are the same phase, DG-CC was selected as a typical sample for XPS analysis. In the survey XPS spectrum (Fig. S2a), the peaks of O 1 s, C 1 s, Co 2p are clearly observed, revealing the coexistence of O, C, and Co elements. The Co $2p_{1/2}$ and Co $2p_{3/2}$ peaks located at 797.9 and 782.5 eV with two prominent shake-up satellite peaks at 802.7 and 787.4 eV (Fig. S2d), respectively. A spin-orbital splitting of 15.4 eV between the Co $2p_{1/2}$ and Co $2p_{3/2}$ peaks is the characteristic feature which indicates the presence of Co^{2+}.

Figure 3. Schematic illustration of the as-synthesized DG-CC, EG-CC and DW-CC

Cyclic voltammetry (CV) is often used to observe the electrochemical reaction potential and speculate the species change during the reaction. CV curves of the first five cycles of DG-CC, EG-CC and DW-CC are shown in Fig. 4(a-c), in which the three kinds of cobalt carbonate have basically similar peaks. In the first cycle, a sharp anode peak at 0.6–0.7 V are observed for the three $CoCO_3$ samples, corresponding to the formation of a solid electrolyte interface (SEI) and the reduction of Co^{2+} (Eq. (1)). Then, the reduction peak splits into two main peaks centered at around 1.0 and 0.8 V in the following cycles, which is attributed to the reduction of Co^{2+} to Co^0 and C^{4+} to lower valence C in CO_3^{2-} (Eq. (2)), respectively [17]. Two main anodic peaks of the three $CoCO_3$ samples are observed at around 1.2 and 1.9 V, which is attribute to the oxidation of low-valence C (C^{x-}) and Co^0, respectively. It can be noted that there is a small

oxidation peak in the CV curves of the three $CoCO_3$ materials at ~ 2.6 V during charging process (Fig. S5, supporting information), corresponding to the reversible oxidation Co(II)/Co(III), which is coincide with the previous reports [15]. It can be noted that the peaks corresponding to Eq. (2) is relatively inconspicuous in the curves of DW-CC implying the reaction is not sufficient.

To further evaluate the lithium storage properties of the DG-CC, EG-CC and DW-CC, cycling tests of the three $CoCO_3$ samples are carried out. Discharge-charge profiles in Fig. 4(d) revealed that the initial discharge/charge capacities at 0.1 A/g for DG-CC, EG-CC and DW-CC are 1478.6/1054.6, 1748.0/1168.5 and 1512.9/1116.9 mAh/g, respectively, and the corresponding Coulombic efficiencies (CEs) are 71.32%, 66.84% and 73.82%. The initial irreversible capacity loss is mainly attributed to the formation of the SEI layer. According to the initial discharge capacity, it can be inferred that 4.7–5.2 Li per $CoCO_3$ was released in the first cycles. In terms of capacity, this value indicates that the traditional conversion reaction is not the only one providing capacity. This result is consistent with the analysis in CV curves. As shown in Fig. 4(e), cobalt carbonates are measured at 0.1 A/g during 200 cycles. In the first 20 cycles, the specific capacity of the three materials decrease rapidly due to the structural adjustment due to volume expansion, and the charge capacities for DG-CC, EG-CC and DW-CC are 904.3, 861.5, 612.1 mAh/g, respectively. Then, the curves tend to be stable and the value of CEs are close to 100% in the following cycle. In the latter half of the cycle process, the specific capacity of the three materials began to rise which may due to the growth of a polymeric gel-like film originating from kinetic activation of the electrode [32]. After 200 cycles, the discharge/charge capacities for DG-CC, EG-CC and DW-CC achieved 960.0/957.2, 857.5/851.9 and 829.6/821.6 mAh/g, respectively. Rate performance of DG-CC, EG-CC and DW-CC is shown in Fig. 4(f). The sample DG-CC delivers the highest capacity with average specific capacity of 1014, 841, 711, 595, 476 mAh/g at current densities of 0.1, 0.2, 0.5, 1, 2 A/g, respectively. When the current density returns to 0.1 A/g, the specific capacity of DG-CC returns to 889 mAh/g. Finally, the sample DG-CC is cycled at a current density of 0.5 A/g, in which the cell maintains at about 660 mAh/g. While for the EG-CC and DW-CC, they deliver lower specific capacities than DG-CC with the increased current densities, demonstrating a gradient relationship (DG-CC > EG-CC > DW-CC). the optimal particle size and high specific surface area, which is conducive to the sample DG-CC participating in the electrochemical reactions.

Most important, the three $CoCO_3$ samples also showed excellent cycle stabilities at a large current density. After the activation for initial 3 cycles at 0.1 A/g and then tested at 1 A/g, the specific capacity goes through the process of rising in the beginning and then generally stable (Fig. 4g). The specific discharge/charge capacity of DG-CC, EG-CC and DW-CC is 692.6/690.7, 383.1/382.8, 295.6/295.0 mAh/g after 1000 cycles, respectively. Generally, DG-CC shows the best cycle performance, which is attributed to the highest specific capacity among the three samples. Based on the stable reversible capacity of the 20th cycle, the capacity retention of DG-CC is 92.45%, indicating that the material has a very stable capacity performance. Comparison of our $CoCO_3$ samples and other previous anode materials in which cobalt carbonate is the main component are summarized in Fig. 4(h) and Table S1 (Supporting Information). The reference points of green, orange, purple and blue in Fig. 4(h) correspond to cobalt

carbonates of pure, compounding, doped, and both doped and compounding, respectively. The ability of DG-CC to withstand repeated charge and discharge under 1 A/g is better than that of most cobalt carbonate materials, and the capacity of DG-CC at 1 A/g even exceeds the samples compounding with other conductive carbon or doped materials. At the same time, the initial Coulombic efficiency of the DG-CC (71.32%) prepared in this study is also at the upstream level. All of the above results show the superiority of DG-CC as an anode material for lithium-ion battery.

To further analysis the performance difference of the three materials in the 1000 cycles, differential charge versus voltage plots and their corresponding charging curves are conducted to describe the voltage platform and potential change of electrochemical reaction at 1 A/g. The corresponding dQ/dV curves of the three samples are shown in Fig. 5(a). Within the 20th and 1000th cycle, three peaks at ~ 1.3, ~ 2.0 and ~ 2.5 V reveal a three-step electrochemical reaction which is consistent with the CV curves in Fig. 4a-c. Therefore, the voltage can be divided into three regions. *Region 1* from 0 to 1.63 V corresponds to the oxidation of C^{x-}. *Region 2* from 1.63 to 2.26 V corresponds to the oxidation of Co^0, and *region 3* from 2.26 to 3 V corresponds to the transition of Co^{2+}/Co^{3+} according to the result of CV curves. Based on the charge profiles in Fig. 5(b), different voltage ranges correspond to different capacity contributions. The concrete capacity contribution in different regions of the three materials in different cycles is summarized in Table S2 (Supporting Information) and further expressed as Fig. 5(c). At the beginning of the cycle, there is little difference between DG-CC and EG-CC in performance, but the difference is obvious when reach 1000th cycle. For DG-CC, capacity contributed from three regions is similar between the 20th and 1000th, respectively. However, the capacity provided by these three reactions for EG-CC and DW-CC are greatly reduced compared with DG-CC, suggests that DG-CC has stronger structural stability. Except for the absolute value of capacity, Fig. 5(d) further shows the contribution ratio statistics of different regions. Compared with the case at the 20th cycle, it is obvious that the main reason for capacity declination at the 1000th cycle is the decrease of capacity contribution of *regions 1* and *2*. The decrease in reversibility may be due to the structural instability caused by the repeated volume changes during cycling. Theoretically, Eqs. (1) and (2) involve more lithium ions, while the transition of Co^{2+}/Co^{3+} in *region 3* only corresponds to 1 equivalent lithium ion. Therefore, the volume effect is more serious in *region 1* and *2*. What's more, once the previous reaction becomes inadequate, the remaining reactants in the subsequent cycle will reduce. This kind of chain effect makes the capacity continue to decline. However, DG-CC shows better stability than EG-CC and DW-CC, which may indicate its structural superiority. The particle size and pore size brought by different solvents should be the key to affect the electrochemical performance.

To further confirm the above conjecture, the morphology of the three kinds of electrodes before and after 1000 cycles is displayed in Fig. 6. The typical particles are selected in the macro morphology as the specimens for analysis which are shown in the upper-right corners of each images. Particles in fresh electrodes of DG-CC, EG-CC and DW-CC distribute uniformly across the whole film surfaces (Fig. 6a-c). The smaller nanoparticles distributed between these $CoCO_3$ particles correspond to the conductive agent. After 1000 discharge-charge cycles, apparently, pulverization is observed on EG-CC and DW-CC particles

(Fig. 6e-f). As is known to all, conversion-type anode materials suffer from relatively large volume change (< 200%) during repeated cycles [5]. Nevertheless, the particles of DG-CC maintain the integrity of morphology (Fig. 6d), which is attributed to the proper sizes of both primary particles and pore sizes of DG-CC. Small primary particles is beneficial to distribute the strain evenly in all regions of the material. Meanwhile, as shown in Fig. 7, appropriate pore size can accommodate these volume changes, so that the secondary particles will not collapse and effectively reduce the loss of active materials. The structure advantage of DG-CC prevents it from falling into the chain effect mentioned above during a long cycle process, which induced by the initial solvent control.

The superiority of morphology of DG-CC is also reflected in the impedance information. Nyquist plots of freshly assembled cells with the active substances of DG-CC, EG-CC and DW-CC are shown in Fig. 8(a), and the data is fitted by the equivalent circuit exhibited in Fig. 8(b). R_s represents the ohmic resistance of the battery. R_{ct} and Z_w (Warburg impedances) describe the resistance of charge transfer and mass transfer, respectively. The specific values of these parameters obtained by fitting are set out in Table S3 (Supporting Information). It is observed that from the Fig. 8(b) that there is almost no difference in the R_s of the cells made by the three $CoCO_3$ samples before cycle. However, DG-CC has the lowest R_{ct}, while DW-CC has the opposite, which further proofs the faster reaction kinetics of DG-CC. Applied by impedance analysis, the change of DG-CC electrode during the cycles was studied. Nyquist plots of DG-CC after the 30th, 90th, 120th and 200th cycle at 1 A/g are displayed in Fig. 8(c). The variation of impedance is summarized in Fig. 8(d) and Table S4 (Supporting Information). From the beginning to the 200th cycle, both R_{SEI} (SEI layer resistances) and R_{ct} has an upward trend in the early stage which may be due to the structural instability caused by volume change. Nevertheless, R_{SEI} and R_{ct} decline rapidly after 90 cycles suggest that the negative effect of electrode structure change disappeared and thus brought about enhanced charge-transport kinetics [8, 33]. It's not difficult to recognize that this result is consistent with the phenomenon that the specific capacity decreases first and then increases during the cycle process (Fig. 4g).

4. Conclusions

In summary, three $CoCO_3$ particles with comparable structures were successfully prepared by facile solvothermal method using different solvents, and results show that the solvent has a significant effect on the morphology of $CoCO_3$. Due to the good matching relationship between particle and pore sizes, DG-CC shows excellent electrochemical performance. When tested at 0.1 A/g, the DG-CC can achieve the capacity of 957.2 mAh/g after 200 cycles. Besides, under the high current density as 1 A/g for 1000 cycles, DG-CC also showed a high specific capacity of 690.7 mAh/g, and corresponding capacity retention could reach 92.45%. The stable particle structure of DG-CC ensures its performance stability in the process of high current circulation. Further analysis shows that the capacity provided by different electrochemical reactions and DG-CC possesses enhanced charge-transport kinetics. The above work shows that reliable cobalt carbonate anode materials can be obtained by simple solvent selection. We

hope that our work could provide reference for further studies in the structural design of $CoCO_3$ or other anode materials.

Declarations

Acknowledgments

This work was supported by the National Natural Science Foundation of China (NSFC) (51772060, 51372052, 51672059, 51621091 and 51902102).

Electronic Supplementary Material

Supplementary material of this work is available in the online version of this article at https://doi.org/10.1007/s40145-...

References

1. Li M, Lu J, Chen Z, Amine K (2018) 30 Years of Lithium-Ion Batteries. Adv Mater 30:1800561. https://doi.org/10.1002/adma.201800561
2. Zeng X, Li M, Abd El-Hady D, Alshitari W, Al-Bogami AS, Lu J, Amine K (2019) Commercialization of Lithium Battery Technologies for Electric Vehicles. Adv Energy Mater 9:1900161. https://doi.org/10.1002/aenm.201900161
3. https://doi/10.1021/acs.chemrev.8b00422
   Winter M, Barnett B, Xu K, Batteries BLiI, Chem. Rev 118 (2018) 11433 – 11456. https://doi/10.1021/acs.chemrev.8b00422
4. Ely DR, Garcia RE (2013) Heterogeneous Nucleation and Growth of Lithium Electrodeposits on Negative Electrodes. J Electrochem Soc 160:A662–A668. https://doi 10.1149/1.057304jes.
5. Poizot P, Laruelle S, Grugeon S, Dupont L, Tarascon J-M (2000) Nano-Sized Transition-Metal Oxides as Negative-Electrode Materials for Lithium-Ion Batteries. Nature 47:469–499. https://doi.org/10.1038/35035045
6. Chu Y, Guo L, Xi B, Feng Z, Wu F, Lin Y, Liu J, Sun D, Feng J, Qian Y, Xiong S (2018) Embedding $MnO@Mn_3O_4$ Nanoparticles in an N-Doped-Carbon Framework Derived from Mn-Organic Clusters for Efficient Lithium Storage. Adv Mater 30:1704244. https://doi.org/10.1002/adma.201704244
7. Zhang R, Huang X, Wang D, Hoang TKA, Yang Y, Duan X, Chen P, Qin LC, Wen G (2018) Single-Phase Mixed Transition Metal Carbonate Encapsulated by Graphene: Facile Synthesis and Improved Lithium Storage Properties. Adv Funct Mater 28:1705817. https://doi.org/10.1002/adfm.201705817
8. Zhao S, Wang Z, He Y, Jiang H, Harn YW, Liu X, Su C, Jin H, Li Y, Wang S, Shen Q, Lin Z, A Robust Route to $Co_2(OH)_2CO_3$ Ultrathin Nanosheets with Superior Lithium Storage Capability Templated by Aspartic Acid-Functionalized Graphene Oxide, Adv Energy Mater 9 (2019) 1901093. https://doi.org/10.1002/ aenm.201901093

9. Lu Y, Yu L, Lou XW, Nanostructured Conversion-Type Anode Materials for Advanced Lithium-Ion Batteries, Chem 4 (2018) 972–996. https://doi.org/10.1016/ j.chempr. 2018.01.003
10. Mei J, Liao T, Kou L, Sun Z (2017) Two-Dimensional Metal Oxide Nanomaterials for Next-Generation Rechargeable Batteries. Adv Mater 29:1700176. https://doi.org/10.1002/adma.201700176
11. Reddy MV, Subba Rao GV, Chowdari BVR (2013) Metal Oxides and Oxysalts as Anode Materials for Li Ion Batteries. Chem Rev 113:5364–5457. https://doi.org/10.1021/cr3001884
12. Li J, Li M, Guo C, Zhang L, Recent Progress and Challenges of Micro-/Nanostructured Transition Metal Carbonate Anodes for Lithium Ion Batteries, Eur J Inorg Chem (2018) 4508–4521. https://doi.org/10.1002/ejic.201800853
13. Aragón MJ, Pérez-Vicente C, Tirado JL, Submicronic Particles of Manganese Carbonate Prepared in Reverse Micelles: A New Electrode Material for Lithium-Ion Batteries, Electrochem Commun 9 (2007) 1744. https://doi.org/10.1016/j.elecom. 2007.03.031
14. Wang L, Tang W, Jing Y, Su L, Zhou Z (2014) Do Transition Metal Carbonates Have Greater Lithium Storage Capability Than Oxides? A Case Study of Monodisperse $CoCO_3$ and CoO Microspindles. ACS Appl Mater Interfaces 6:12346–12352. https://doi.org/10.1021/am5021233
15. Ding Z, Qin X, You C, Wu M, He Y, Kang F, Li B (2018) Different Solid Electrolyte Interface and Anode Performance of $CoCO_3$ Microspheres Due to Graphene Modification and $LiCoO_2$||$CoCO_3$@rGO Full Cell Study. Electrochim Acta 270:192–204. https://doi.org/10.1016/j.electacta.2018.03.041
16. Zhao Z, Wan Z, Deni DK, Su X, Zhan J, Hou L, Zhang X, Yuan C, Intrinsic Lithium Storage Mechanisms and Superior Electrochemical Behaviors of Monodispersed Hierarchical $CoCO_3$ Sub-Microspheroids as a Competitive Anode towards Li-Ion Batteries, Electrochim Acta 307 (2019) 20–29. https://doi.org/ 10.1016/j.electacta. 2019.03.171
17. Ding Z, Yao B, Feng J, Zhang J (2013) Enhanced Rate Performance and Cycling Stability of a $CoCO_3$-Polypyrrole Composite for Lithium Ion Battery Anodes. J Mater Chem A 1:11200–11209. https://doi.org/10.1039/C3TA12227A
18. Shao L, Ma R, Wu K, Shui M, Lao M, Wang D, Long N, Ren Y, Shu J (2013) Metal Carbonates as Anode Materials for Lithium Ion Batteries. J Alloys Comp 581:602–609. https://doi.org/10.1016/j.jallcom.2013.07.167
19. Huang G, Xu S, Yang Y, Sun H, Li Z, Chen Q, Lu S (2014) Micro-Spherical $CoCO_3$ Anode for Lithium-Ion Batteries. Mater Lett 131:236–239. https://doi.org/10.1016/j.matlet.2014.05.208
20. 10.1002/ cssc.201700171
Li HY, Tseng CM, Yang CH, Lee TC, Su CY, Hsieh CT, Chang JK, Eco-Efficient Synthesis of Highly Porous $CoCO_3$ Anodes from Supercritical CO_2 for Li^+ and Na^+ Storage, ChemSusChem 10 (2017) 2464–2472. https://doi.org/10.1002/ cssc.201700171
21. Shi S, Zhang M, Liu Y, Hua X, Guo H, Yang G, Efficient Construction of a $CoCO_3$/Graphene Composite Anode Material for Lithium-Ion Batteries by Stirring Solvothermal Reaction, Ceram Int 44 (2018) 3718–3725. https://doi.org/10.1016/ j.ceramint.2017.11.152

22. Zeng T, Zhang C, Facile-Synthesized Amorphous $CoCO_3$ for High-Capacity Lithium-Ion Battery Anode, Ionics 25 (2019) 4149–4159. https://doi.org/10.1007/ s11581-019-03006-4
23. Su L, Zhou Z, Qin X, Tang Q, Wu D, Shen P (2013) $CoCO_3$ Submicrocube/ Graphene Composites with High Lithium Storage Capability. Nano Energy 2:276–282. https://doi.org/10.1016/j.nanoen.2012.09.012
24. Lu Z, Wang H, Zhou T, Ma C, Yin F, Jiang X, Yang G (2018) $CoCO_3$ Micrometer Particles Stabilized by Carbon Nanofibers Networks as Composite Electrode for Enhanced Rate and Cyclic Performance of Lithium-Ion Batteries. Electrochim Acta 270:22–29. https://doi.org/10.1016/j.electacta.2018.03.081
25. Zhao S, Wei S, Liu R, Wang Y, Yu Y, Shen Q (2015) Cobalt Carbonate Dumbbells for High-Capacity Lithium Storage: A Slight Doping of Ascorbic Acid and an Enhancement in Electrochemical Performances. J Power Sources 284:154–161. https://doi.org/10.1016/j.jpowsour.2015.03.016
26. Yin J, Ding Z, Lei D, Tan L, Deng J, Li B, He YB, Zn-Substituted $CoCO_3$ Embedded in Carbon Nanotubes Network as High Performance Anode for Lithium-Ion Batteries, J Alloy Compd 712 (2017) 605–612. https://doi.org/10.1016/ j.jallcom.2017.04.055
27. Jin Y, Zhu B, Lu Z, Liu N, Zhu J (2017) Challenges and Recent Progress in the Development of Si Anodes for Lithium-Ion Battery. Adv Energy Mater 7:1700715. https://doi.org/10.1002/aenm.201700715
28. Zhao Y, Wang LP, Sougrati MT, Feng Z, Leconte Y, Fisher A, Srinivasan M, Xu Z (2017) A Review on Design Strategies for Carbon Based Metal Oxides and Sulfides Nanocomposites for High Performance Li and Na Ion Battery Anodes. Adv Energy Mater 7:1601424. https://doi.org/10.1002/aenm.201601424
29. Deng D, Kim MG, Lee JY, Cho J (2009) Green Energy Storage Materials: Nanostructured TiO_2 and Sn-Based Anodes for Lithium-Ion Batteries. Energy Environ Sci 2:818–837. https://doi.org/10.1039/B823474D
30. Wang S, Yang Y, Dong Y, Zhang Z, Tang Z (2019) Recent Progress in Ti-Based Nanocomposite Anodes for Lithium Ion Batteries. J Adv Ceram 8:1–18. https://doi.org/10.1007/s40145-018-0292-2
31. Zhou L, Zhang K, Hu Z, Tao Z, Mai L, Kang Y-M, Chou S-L, Chen J (2018) Recent Developments on and Prospects for Electrode Materials with Hierarchical Structures for Lithium-Ion Batteries. Adv Energy Mater 8:1701415. https://doi.org/10.1002/aenm.201701415
32. Laruelle S, Grugeon S, Poizot P, Dollé M, Dupont L, Tarascon JM, On the Origin of the Extra Electrochemical Capacity Displayed by MOÕLi Cells at Low Potential, J Electrochem Soc 149 (2002) A627–A634. https://doi.org/10.1149/ 1.1467947
33. Zhang R, Wang D, Qin LC, Zhou Y, Wen G, Pan H, Zhang Y, Tian N, Huang X, $MnCO_3$/Mn_3O_4/Reduced Graphene Oxide Ternary Anode Materials for Lithium-Ion Batteries: Facile Green Synthesis and Enhanced Electrochemical Performance, J Mater Chem A 5 (2017) 17001–17011. https://doi.org/10.1039/ C7TA02874A

Figures

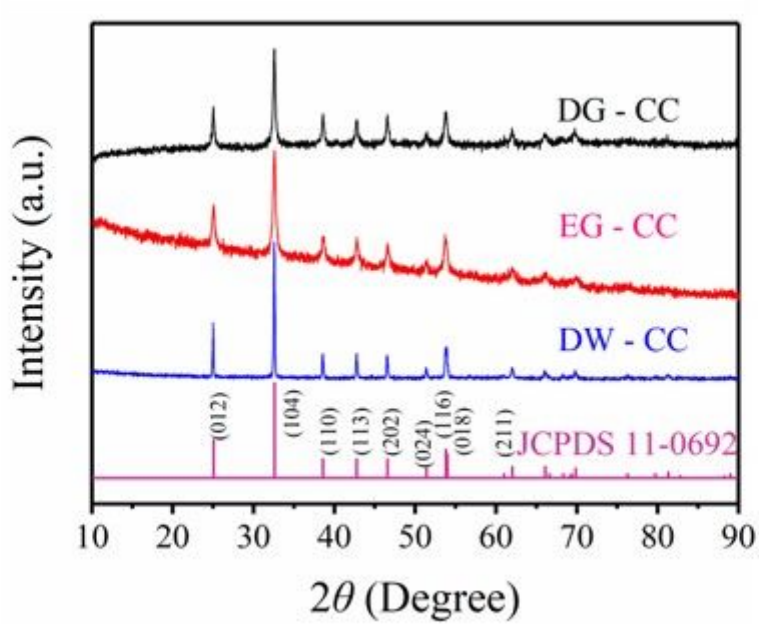

Figure 1

XRD patterns of DG-CC, EG-CC and DW-CC.

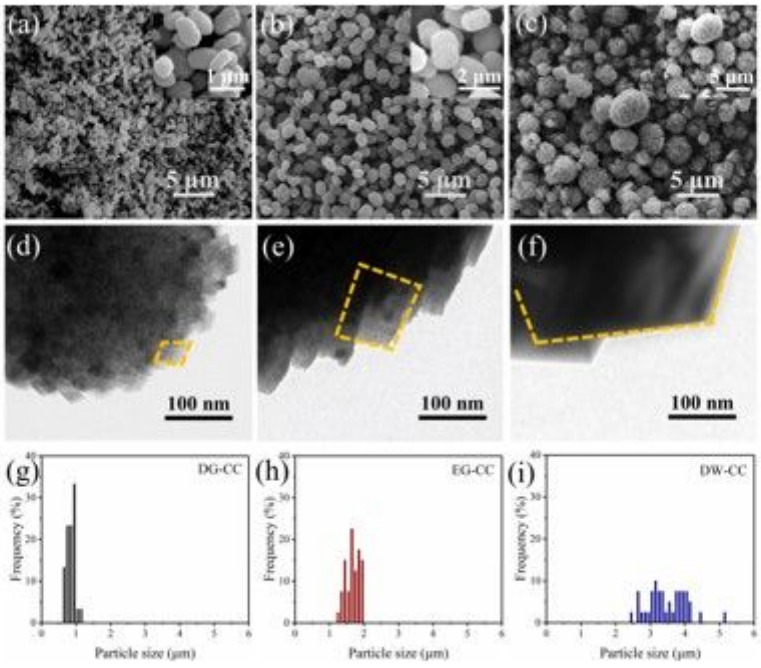

Figure 2

SEM images, TEM images in details and particle size distribution of (a, d, g) DG-CC, (b, e, h) EG-CC and (c, f, i) DW-CC.

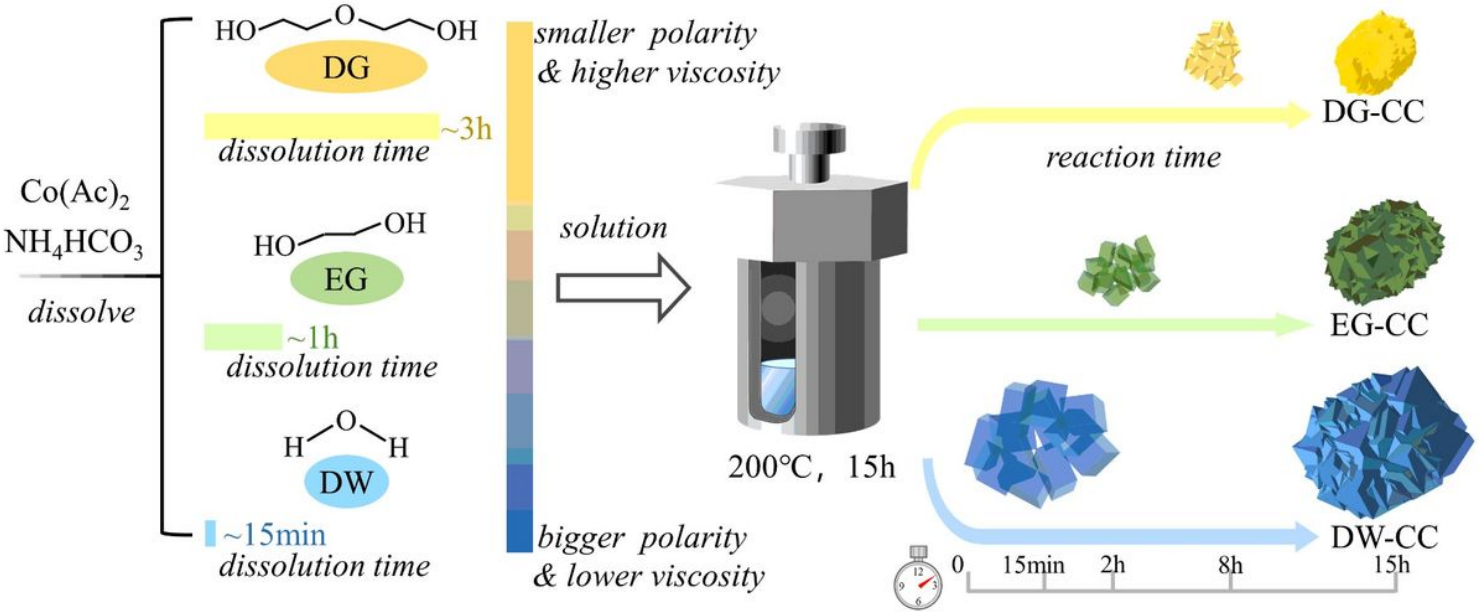

Figure 3

Schematic illustration of the as-synthesized DG-CC, EG-CC and DW-CC

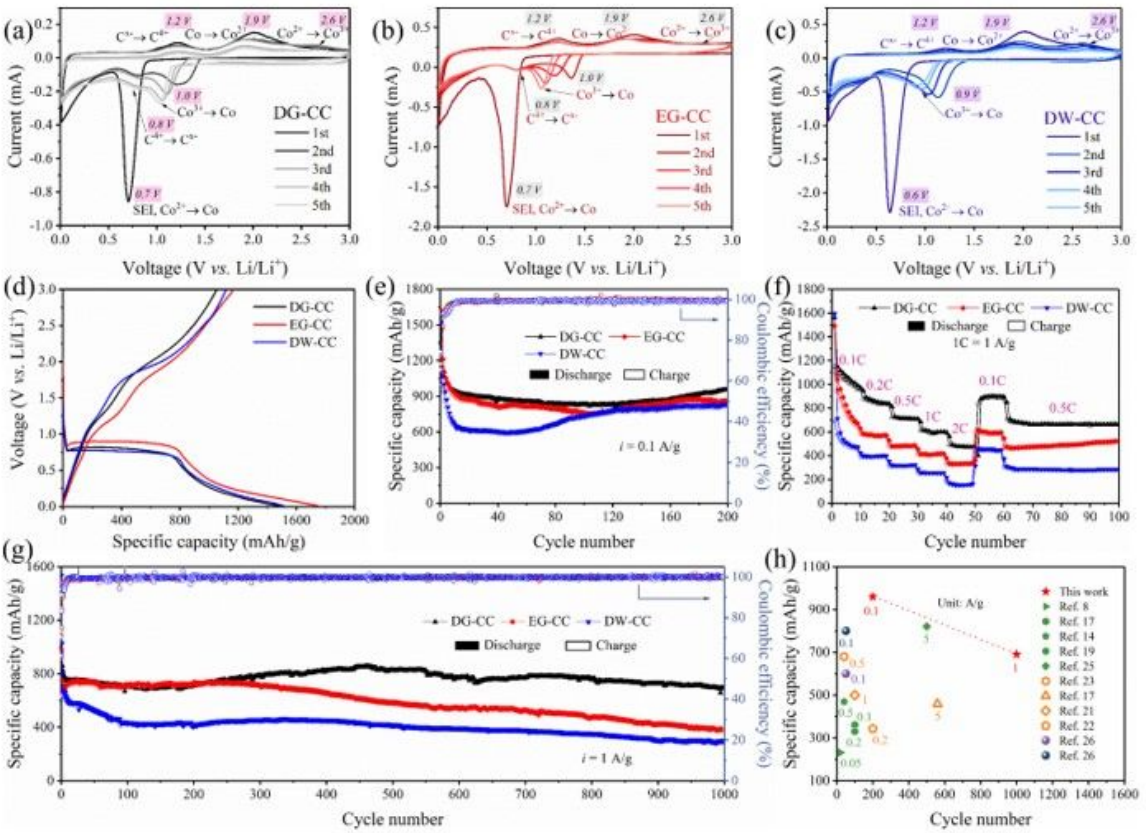

Figure 4

CV curves of (a) DG-CC, (b) EG-CC and (c) DW-CC; (d) Galvanostatic discharge-charge profiles for the first cycle, (e) Cycling performance at 0.1 A/g, (f) Rate performance and (g) Long cycle performance at 1 A/g of the three CoCO3 samples; (h) Comparison of our DG-CC with previous works.

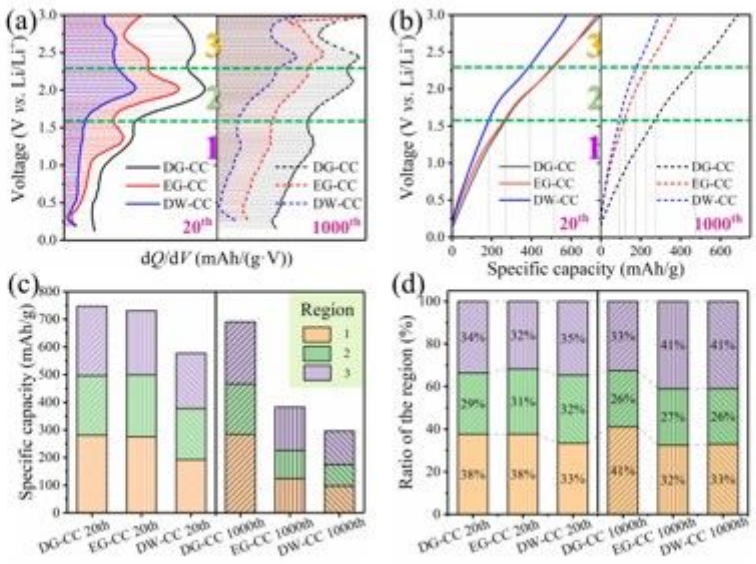

Figure 5

(a) Differential charge versus voltage plots based on 20th and 1000th charging process and their (b) Corresponding charge profiles; (c) Capacity contribution and (d) The corresponding ratio of each region in the 20th and 1000th cycle for DG-CC, EG-CC and DW-CC.

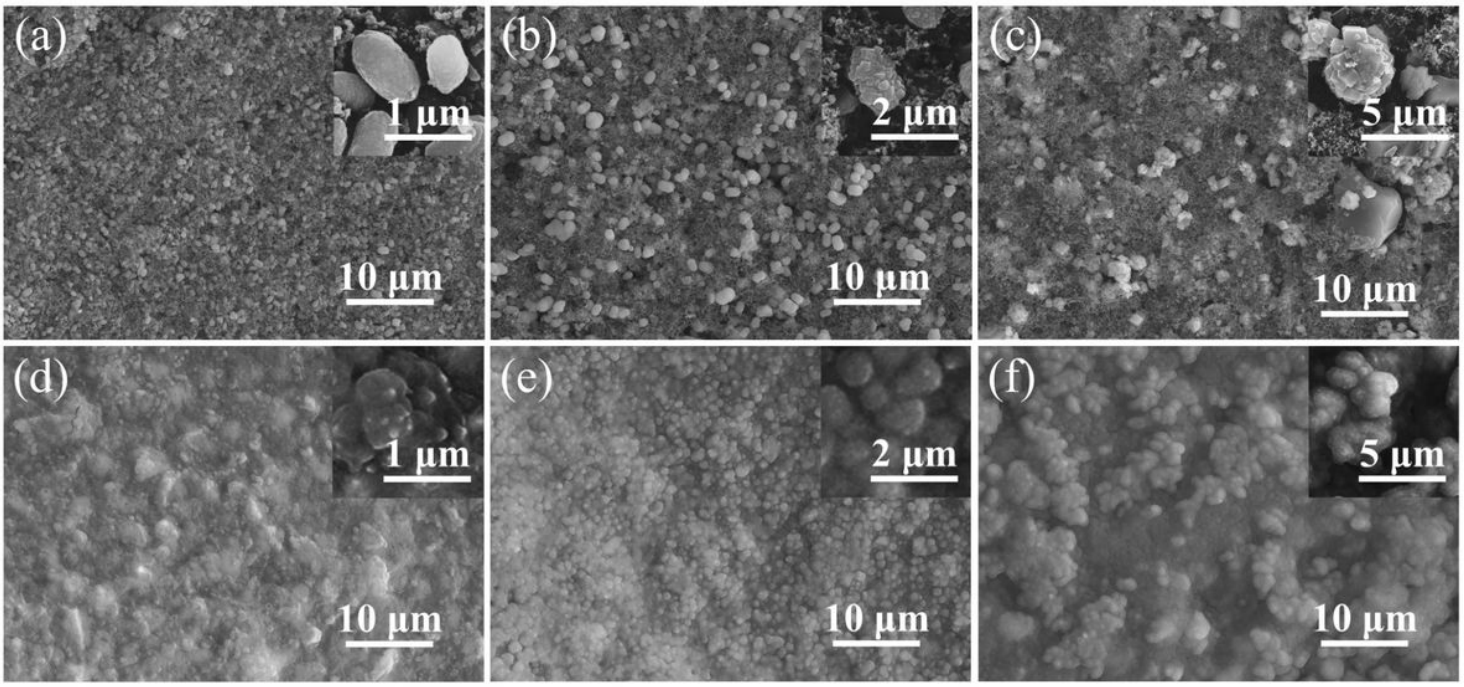

Figure 6

SEM images of (a-c) uncycled and (d-e) cycled electrodes after 1000 cycles at 1 A/g for DG-CC, EG-CC and DW-CC.

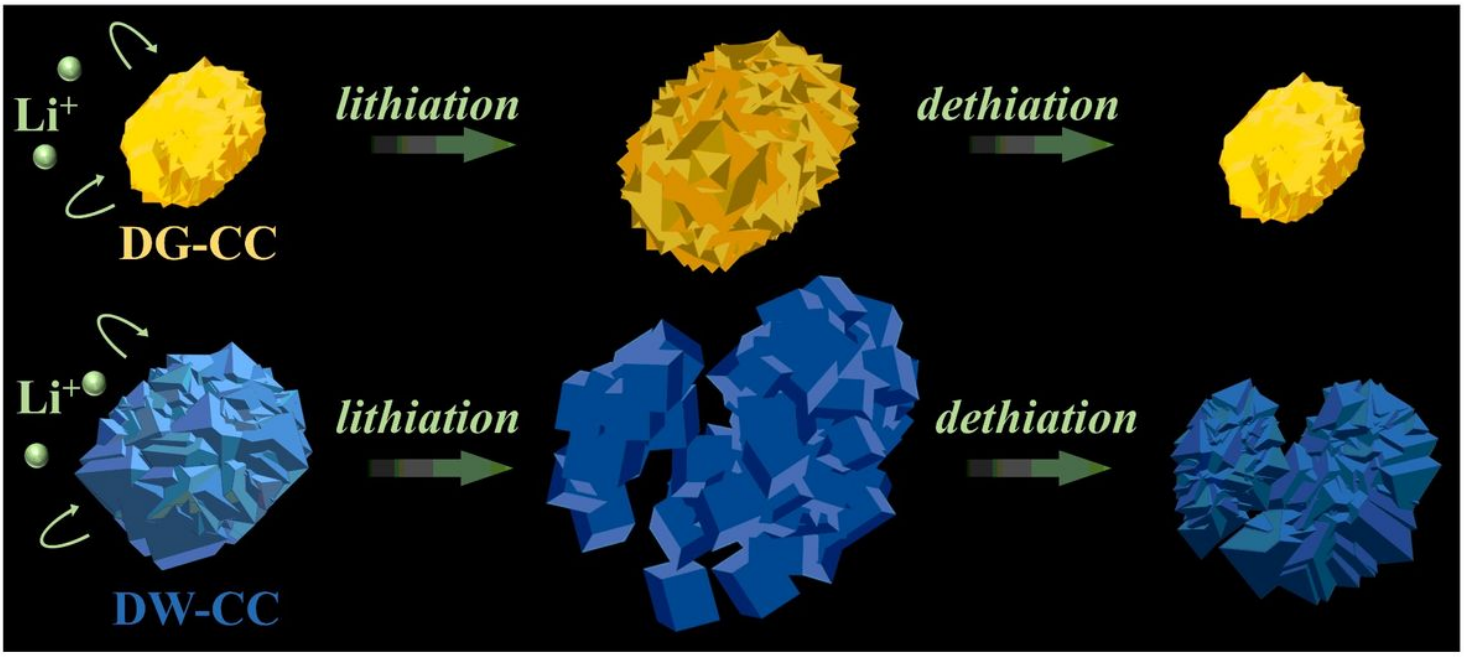

Figure 7

Schematic diagram of the morphologic change of cobalt carbonate particles during liathiation and deliathiation

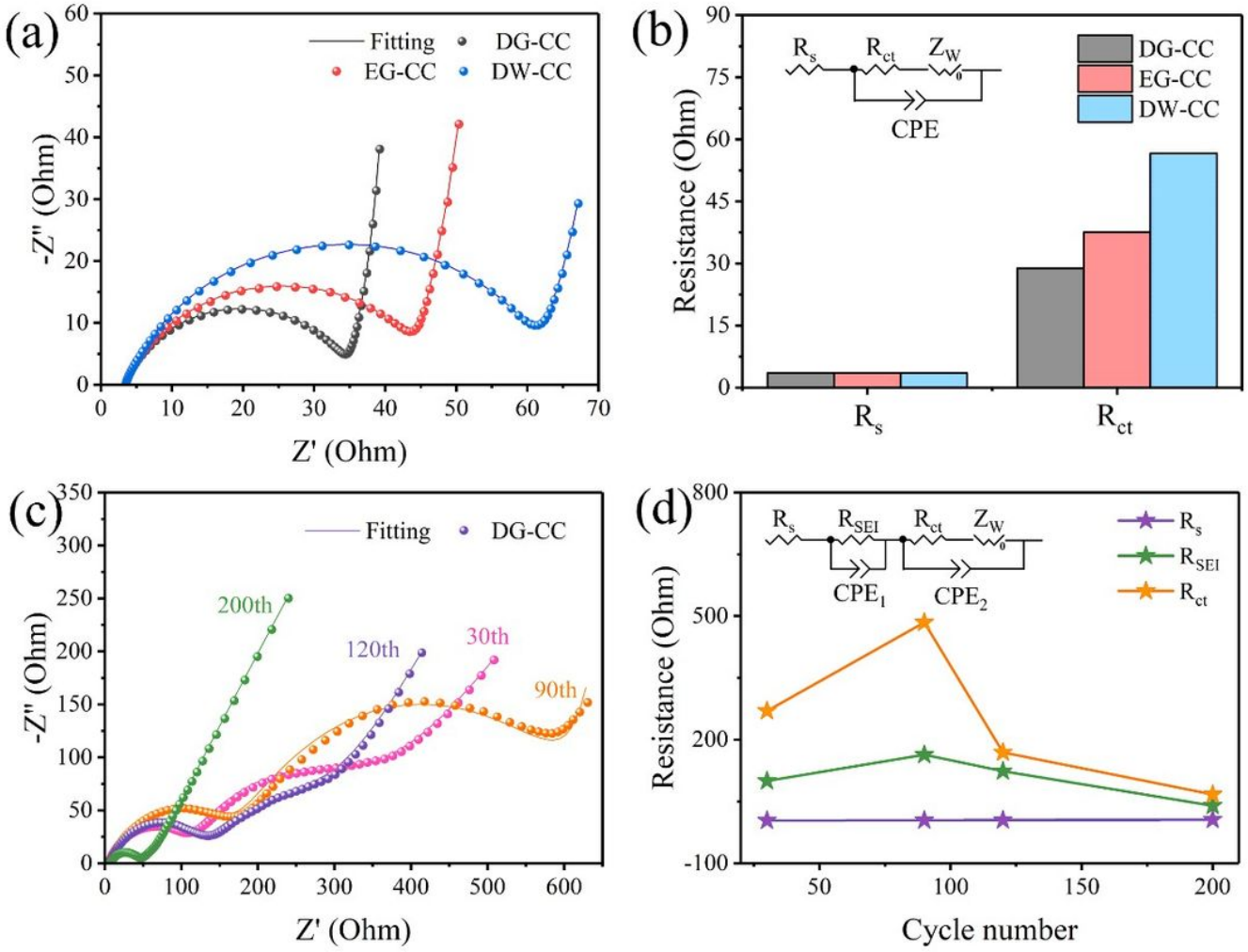

Figure 8

(a) Nyquist plots of freshly assembled cells of DG-CC, EG-CC and DW-CC and their (b) Corresponding comparisons of fitting parameters; (c) Nyquist plots of DG-CC after different cycles and (d) The variation of different resistance with cycle number.

Supplementary Files

This is a list of supplementary files associated with this preprint. Click to download.

- Supportinginformation.docx